



Thermal behavior and antibacterial studies of a carbonate Mg–Al-based layered double hydroxide (LDH) for in vivo uses

Anna Maria Cardinale¹ · Stefano Vecchio Cipriotti² · Marco Fortunato¹ · Michelina Catauro³

Received: 3 December 2021 / Accepted: 20 March 2022
© The Author(s) 2022

Abstract

The goal of this work is to study the thermal behavior and the antibacterial properties of a MgAl-CO₃ layered double hydroxide (LDH), which demonstrated high efficiency in removing chromium (VI) from contaminated industrial wastewater. The compound has been synthesized via co-precipitation route (direct method) followed by hydrothermal treatment, obtaining nanoscopic crystallites with a partially disordered (turbostratic) structure. After its synthesis, the compound was characterized by means of X-ray powder diffraction, field emission scanning electron microscope, inductively coupled plasma atomic emission spectroscopy and analysis and Fourier transform infrared spectroscopy. On the other hand, with the view to check the drug delivery and surgical tools usage of MgAl-CO₃, antibacterial tests, performed according to the Kirby–Bauer method, revealed the inability the growth of the pathogenic bacterial strains. Thermogravimetry and differential thermal analysis revealed that evolution of water from the material occurs in two stages upon heating and a noticeable interaction takes place between water (in the vapor phase) and MgAl-CO₃. Kinetic analysis of both steps provides almost constant values of activation energy, with the following average values in the range $0.1 < a < 0.9$: $E_1 = (66 \pm 9) \text{ kJ mol}^{-1}$; $E_2 = (106 \pm 7) \text{ kJ mol}^{-1}$. Finally, prediction of reasonable reaction times extrapolated at 25 and 37 °C has been made from kinetic parameters of the first step, while almost unrealistic reaction time values were determined using the same procedure with kinetic parameters related to the second step.

Keywords LDHs · TGA · DTA · XRPD · FESEM · FT-IR · KAS method · Incremental isoconversional method · Antibacterial activity

Introduction

Nowadays, one of the most participate scientific and technological challenge is the study of promising materials with tunable properties suitable for different applications. In this scenario, layered double hydroxides (LDHs) play a role of leading actors owing to their 2D layered structure and the

possibility of building them (fine tuning their specific properties) by combining different cations and anions.

The structure of LDHs can be derived from that of *brucite*, Mg(OH)₂, consisting of layers of Mg²⁺ cations octahedrally coordinated with six hydroxide anions; in an LDH, the replacement of a fraction of the Mg²⁺ ions with a trivalent cation occurs, thus leading to a positive charge on the surface, which necessitates a balancing anion at the interlayer. These M²⁺/N³⁺(OH)₆ octahedra (where M and N are bivalent and trivalent metals, respectively) form 2D sheets via edge sharing and may be connected sheet to sheet by hydrogen bridge bonding between the hydroxide groups. As the structure, LDHs similarly to hydrotalcite belong to the space group R $\bar{3}$ m-h [1]. LDHs are used in a wide range of applications [2], including catalysis [3], energy conversion and storage [4, 5], remediation [6, 7], electrochemical and drugs delivery purposes [8, 9].

Furthermore, only a deep knowledge of the LDH chemical physical properties can allow to plan and set up the better

✉ Anna Maria Cardinale
cardinal@chimica.unige.it

✉ Stefano Vecchio Cipriotti
stefano.vecchio@uniroma1.it

¹ Dipartimento di Chimica e Chimica Industriale, Università di Genova, Via Dodecaneso 31, 16146 Genova, Italy

² Dipartimento di Scienze di Base ed Applicate per l'Ingegneria, Sapienza Università di Roma, Via del Castro Laurenziano 7, 00161 Roma, Italy

³ Dipartimento di Ingegneria, Università della Campania "Luigi Vanvitelli", Via Roma 29, 81031 Aversa, Italy

compound for each scope. Just for this purpose in this work will be studied a Mg–Al LDHs as far as the structure, the thermal behavior and the biocompatibility are concerned.

The investigated compound is MgAl-CO₃; a carbonate LDH material whose carbonate groups are located between adjacent layers, has been previously used for the removal of sulfate from wastewater [10] and remediation [6], demonstrating to provide a good performance when used with a galvanic plant polluted water. Since Mg–Al-based LDHs also find use in drug delivery and biomedical imaging [9, 11], the knowledge of the antibacterial activity seems to assume, like for bioactive glasses [12, 13], a crucial importance and needs to be further investigated. On the other hand, some of these LDHs may intercalate suitable molecules and a thermal treatment of the so-obtained precursor materials may convert them into very promising oxides or composites [14, 15]. The thermal activation of a LDH by calcination in a wide temperature range that usually is between 300 and 500 °C causes the release of water due to condensation of hydroxyl groups resulting in the formation a mixed metal oxides [16, 17]. Therefore, the knowledge of their thermal behavior is also of paramount importance to select the most appropriate temperature for the thermal treatment [18]. Furthermore, the knowledge of the decomposition step upon heating is fundamental in plan the better compound for the specific usage in surgical equipment and devices. In addition, in recent years the thermal behavior study and the assessment of thermal stability have become crucial issues in the characterization of different classes of materials and nanocomposites via the use of thermal analysis techniques. As a matter of fact, in the last one or two decades these aspects were particularly developed for glasses [19–21], organic–inorganic hybrids [22–26], ceramic and geopolymer materials [27, 28], nanocomposites [29, 30], polysiloxanes [31], analgesics and antibiotics [32] and coordination compounds [33–36].

So, as a continuation of this research, the aim of this study is to investigate the thermal behavior of MgAl-CO₃ prepared via hydrothermal synthesis and characterized by means of several techniques (inductively coupled plasma atomic emission spectroscopy, ICP-AES), Fourier transform infrared spectroscopy (FT-IR), X-ray powder diffraction (XRPD), field emission scanning electron microscopy (FESEM), Kirby–Bauer test). This end was achieved also through thermogravimetry (TG) and differential thermal analysis (DTA), focusing mainly our attention on the potential reversible characteristics of dehydration and the very promising results derived by an isoconversional kinetic analysis of this process.

Experimental

Synthesis

The achievement of the desired LDH stoichiometry and morphology (depending from the perspective of usage) is just a matter of the right combination of different factors: synthesis procedures, pH of the reaction, type of reagents, solvents, temperature and reaction duration. Based on our previous experiences and on the literature [18], the compound has been synthesized by choosing a hydrothermal pathway at 180 °C for 1 h, which leads to a more nanostructured product with respect to the one synthesized for the study reported in [18], and dried overnight at low temperature (80 °C).

To prepare the MgAl-CO₃ LDH, as described by [37], the reagents Al(NO₃)₃·9H₂O (98.8% purity, supplied by VWR CHEMICALS, Leuven, Belgium), Mg(NO₃)₂·9H₂O (98.9% purity, supplied by VWR CHEMICALS, Leuven, Belgium) and urea (99.8 mass% purity, supplied by CARLO ERBA, Milan, Italy) were used. After dissolution of the due amount of the reagents depending on the desired Mg/Al ratio, the reaction was carried out in a Teflon vessel autoclave at 180 °C for 1 h. The obtained white compound was separated from the solution by centrifugation at 7000 rpm for 10 min, repeatedly washed with water and dried in an oven at 60 °C for 24 h. The chemical analyses were performed by inductively coupled plasma atomic emission spectroscopy (ICP-AES) after dissolution of the sample in a concentrated nitric acid solution. A final Mg/Al molar ratio of 2.4 was then obtained for the material investigated.

Characterization

All the samples were characterized by means of several techniques. The ICP-AES measurements were performed using an axially viewed Varian (Springvale, Australia) Vista PRO. The sample introduction system consisted of a glass concentric K-style pneumatic nebulizer (Varian) jointed to a glass cyclonic spray chamber (Varian). In order to compensate for non-spectral interferences, the online internal standardization (4 µg mL⁻¹ Lu standard solution) was applied. All details of the ICP-AES operating parameters are available in a previous study [6]. XRPD patterns were collected to identify the eventual crystalline phase using a X'Pert MPD (Philips, Almelo, Netherland) X-ray powder diffractometers equipped with a Cu anticathode with Cu Kα1 radiation (λ = 1.5406 Å). The indexing of the obtained diffraction data was performed by comparison of signals with those available in the literature

[38] and refined with the Rietveld method, while the lattice parameters of the phases were calculated using the LATCON program [39]. A ZEISS SUPRA 40 V model of the field emission scanning electron microscope (FESEM) was used, where the sample was analyzed by applying an acceleration voltage of 5 kV for 50 s. FT-IR spectra were collected in the usual wavelength range from 4000 to 600 cm^{-1} using a Spectrum 65 FT-IR Spectrometer (PerkinElmer, Waltham, MA, USA) equipped with a KBr beam splitter and a DTGS detector by using an ATR accessory with a diamond crystal. TG/DTA analysis was performed using a LabsysEvo 1600–Setaram; about 20 mg of sample was placed in an open alumina crucible and heated under a flowing Ar atmosphere at 60 mL min^{-1} from 30 to 1250 $^{\circ}\text{C}$ at 5 $^{\circ}\text{C min}^{-1}$ (for the thermal behavior study) and at five different heating rates (1, 3, 5, 7 and 9 $^{\circ}\text{C min}^{-1}$) for computing kinetics analysis. To check the occurrence of a possible interaction between the solid reactant or the solid product and the gaseous product, four different TG experiments have been carried out using different sample masses (about 5, 10, 15 and 20 mg) under a heating rate of 5 $^{\circ}\text{C min}^{-1}$ in a flowing Ar atmosphere at 60 mL min^{-1} from ambient temperature to 320 $^{\circ}\text{C}$.

Antibacterial activity

To evaluate the antibacterial properties of the material, a Kirby–Bauer test was performed as it was recently made for glass hybrid materials [40, 41]. Gram-negative bacteria (–), namely *Escherichia coli* (ATCC 25,922) and *Pseudomonas aeruginosa* (ATCC27853), and gram-positive bacteria (+), as *Staphylococcus aureus* (ATCC 25,923) and *Enterococcus faecalis* (ATTC29212), were grown in the absence and presence of the sample.

Hundred milligrams of powder sample was radiated by UV light for 1 h for sterilization. A bacterial suspension of 10^9 CFU mL^{-1} was obtained by diluting pellet strains in distilled saline water (0.9% NaCl). Then, *E. coli* was plated on TBX (Tryptone Bile X-Gluc) Medium (Liofilchem, Italy), while *S. aureus* was plated on Baird-Parker agar (Liofilchem, Italy), *P. aeruginosa* on Pseudomonas CN agar and, finally, *E. faecalis* on Slanetz Bartley agar base. Except for *E. faecalis*, all media were sterilized up to 120 $^{\circ}\text{C}$ for 15 min. After the occurrence of the sterilization process, a CN pseudomonas supplement was added to Pseudomonas CN agar after cooling up to 45 $^{\circ}\text{C}$. Finally, the powders were placed in the middle of Petri dishes, and then *E. coli* plates were incubated at 44 $^{\circ}\text{C}$ for 24 h, *S. aureus* at 36 $^{\circ}\text{C}$ for 24 h and *E. faecalis* and *P. aeruginosa* plates at 36 $^{\circ}\text{C}$ for 48 h.

The diameter of inhibition halos (IDs) in relation to the Petri plate diameter (PPD) (6 cm) was calculated. Four measurements were carried out for each specimen to obtain

the mean standard deviation. Data are expressed as bacterial viability (BV) (expressed as %) according to Eq. (1):

$$BV = \frac{(PPD - IDs)}{PPD} \times 100 \quad (1)$$

100% BV represents the bacteria viability without samples. The bacterial plating process is shown in Fig. S1 (Supplementary Material).

Theoretical background of kinetic analysis

The reaction rate of each degradation step is expressed by the basic kinetic equation using the following form:

$$d\alpha/dt = k(T) \cdot f(\alpha) \quad (2)$$

where α is the degree of conversion defined as the fractional area of the corresponding DTA or DSC peak associated with the investigated process. Furthermore, k and f are temperature and conversion functions, respectively, where $k(T)$ is a temperature function that may assume different forms (like that of Hartcourt and Esson [42]). The $k(T)$ function is often expressed by the Arrhenius equation ($\ln k(T) = \ln A_k - E/RT$), where A_k and E are the pre-exponential factor and the activation energy, respectively. After some rearrangements, the left-hand side of Eq. (1), being the heating rate β equal to dT/dt , becomes:

$$d\alpha/dt = dT/dt \cdot d\alpha/dT = \beta \cdot d\alpha/dT \quad (3)$$

and, after separating both α and T variables, it yields:

$$d\alpha/f(\alpha) = (A_k/\beta) \cdot \exp(-E/RT)dT \quad (4)$$

By integrating both hand sides of Eq. (4), Eq. (5) can be obtained:

$$\int_0^\alpha d\alpha/f(\alpha) = \int_0^T (A_k/\beta) \cdot \exp(-E/RT)dT \quad (5)$$

The temperature integral in Eq. (5) has no exact but approximate solutions. The so-called integral isoconversional methods can be obtained using the well-known Doyle's approximation [43], based on the general equation:

$$\ln(\beta/T_a^a) = f(1/T\alpha) \quad (6)$$

where at each given degree of conversion a single value of activation energy E is determined from the slope of the linear regression line of Eq. (6) according to the least square method, being $a=2$ for the Kissinger–Akahira–Sunose (KAS) method [44]. The integral isoconversional methods can be considered correct only on assuming that the E values are practically constant over the almost whole range of α values (E depends formally only on the temperature [45–47]).

By contrast, when activation energy varies by more than 20% of the average value, incremental isoconversional methods represent a valuable compromise between the differential (too sensitive toward the experimental noise [48]) and integral ones (not able to handle the conversion dependence of the E values). The incremental isoconversional methods proposed by Simon and co-workers [43, 46] have the advantage that prior to the calculation no transformation can be made on the experimental data, and the objective function (to be minimized) has a physical meaning and is statistically well-grounded. At each given value of α , the values of activation energy and pre-exponential factor are obtained from the slope and intercept of the regression line reported in Eq. (7):

$$\ln \left[\beta / (T_{i+1} - T_i) \right] = -\ln(A) - (E/R) \cdot 2 / (T_{i+1} + T_i) \quad (7)$$

where $A = [g(\alpha_{i+1}) - g(\alpha_i)]/A_k$, being $g(\alpha_{i+1})$ and $g(\alpha_i)$ the values of the integral model function $g(\alpha)$ for two conversion levels α_i and α_{i+1} corresponding to temperatures T_i and T_{i+1} , respectively [45]. The detailed procedure for kinetic analysis adopted in this study has been summarized for the sake of clarity in Fig. S2 (Supplementary Material).

On the other hand, the estimated reaction time can be easily predicted isothermally by summing all the Δt_i time intervals according to Eq. (8) [49]:

$$t_\alpha = \sum_i \Delta t_i = \sum_i A_i \cdot \exp(-E_i/RT) \quad (8)$$

where A_i and E_i are the Arrhenius pair related to the corresponding degree of conversion α .

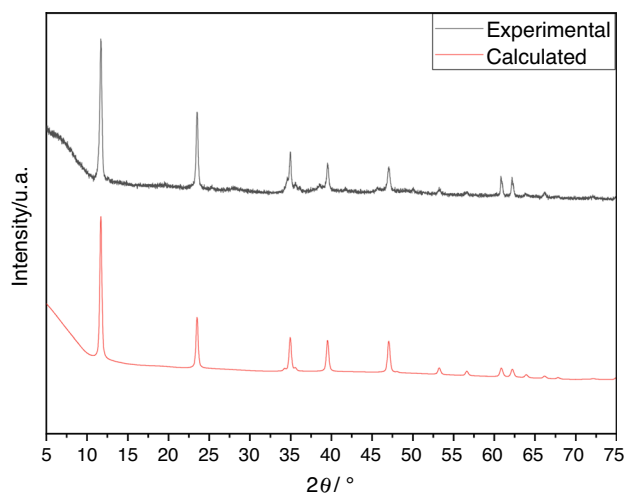


Fig. 1 XRPD patterns of MgAl-CO₃

Results and discussion

Structural (XRDP) and morphological (FESEM) analysis

Figure 1 displays the diffraction patterns of the compound; owing to the synthesis pathway chosen, the carbonate LDH (prepared hydrothermally) is clearly highly crystalline, showing the typical symmetric (003) (006) (110) (113) and asymmetric (015) (018) reflections. The crystal structure was determined by Rietveld refinement with the assistance of the FullProf software package [50], and the cell parameters have been calculated giving the following results: $a = 0.3044(34)$ nm, $c = 2.2712(1)$ nm, $V_{\text{cell}} = 0.1823(1)$ nm³.

The hydroxide layer thickness is approximately evaluated 0.24 nm [51], so the interlayer regions thickness can be estimated 0.51 nm. Figure 2 shows the FT-IR spectrum for the compound, which reveals a high amount of interlayered carbonate. The absorption band due to the vibrational modes of the very symmetric interlayer carbonate results in a single large band at 1347 cm⁻¹, partially overlapped to a slight shoulder at 1440 cm⁻¹ typical for the asymmetric environment of an intercalated carbonate anion.

Further concerning the carbonate signals, going toward the lower wave numbers there are the two absorption bands at 865 and 835 cm⁻¹. The signals at the lowest frequency can be attributed to the cation oxygen bonds vibrations. At 3410 cm⁻¹, there is the broad adsorption band related to the stretching of the OH groups in coordination with the cations [52], followed by the hydrogen bending in the water molecules bonded with carbonate anions in the interlayer at 2979 cm⁻¹. Finally, the angular deformation of the water in the interlayer is responsible for the small narrow signal at 1576 cm⁻¹.

The FESEM image in Fig. 3 shows the micrographic appearance demonstrating that the morphology develops into a microcrystalline flower like structure, as typical in the

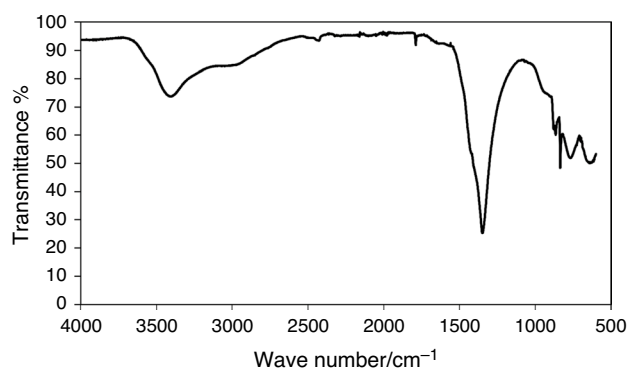


Fig. 2 FT-IR spectra of MgAl-CO₃

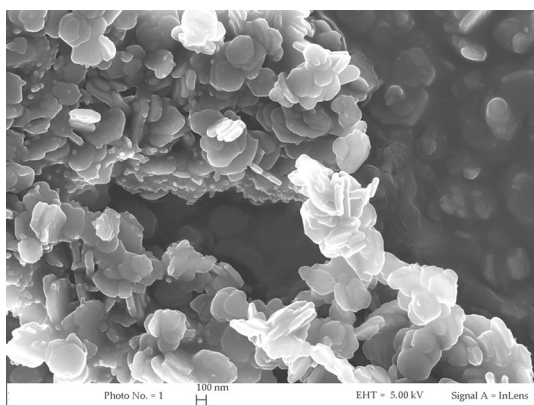


Fig. 3 FESEM images of MgAl-CO₃

hydroxalcite-based compounds prepared via a urea assisted hydrothermal synthesis.

The 3D architecture of the compound is the preferred one for different fields of use, due to a high exchanged surface available [53]. The thickness of the constituent lamellae was estimated between 10 and 20 nm.

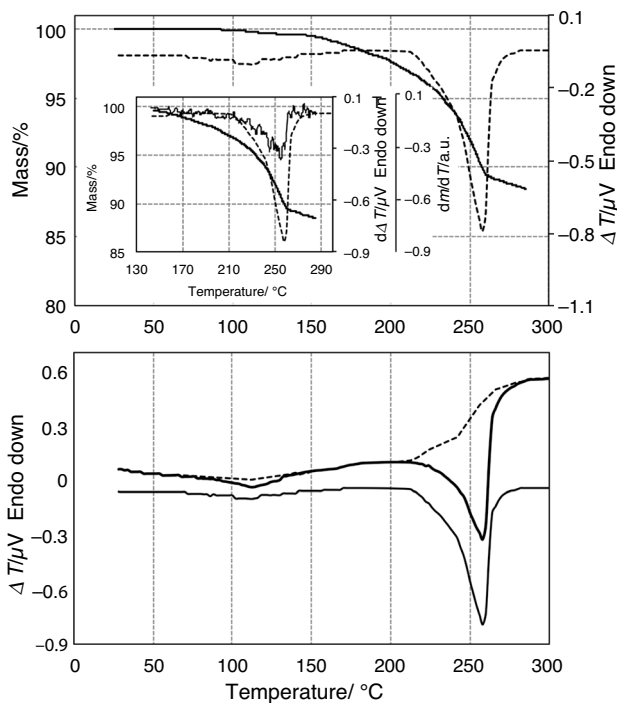


Fig. 4 TG/DTA curves of MgAl-CO₃ (Mg/Al molar ratio=2.4) at 5 °C min⁻¹ under Ar atmosphere (60 mL min⁻¹) after baseline corrections (a) and DTA curves before and after baseline correction (bold and solid lines, respectively)

Thermal behavior study

The TG and DTA curves of MgAl-CO₃ are shown in Fig. 4. Taking into account that the Mg/Al molar ratio is equal to 2.4, the thermal behavior of this material is quite different from that of a MgAl-CO₃ (denoted as material 2) reported in the literature [18], probably because of a different Mg/Al ratio (equal to 4 for material 2).

In particular, Fig. 4a displays the TG and DTA curves after baseline corrections, where Fig. 4b shows DTA raw data (bold line) and the blank curve (dashed line) and the corrected DTA curve (solid line) after a point-by-point subtraction procedure, according to the recommendations for collecting experimental thermal analysis data available in the review published in 2014 by the ICTAC kinetic Project Committee [54]. Two distinct endothermic processes are evident in both TG and DTA curves. No mass loss is observed up to 100 °C (while a sudden mass loss of about 3–4% by mass is detected for material 2 for water physically adsorbed). A small mass loss is found between 100 and 140 °C, associated with a weakly intense, and broad DTA peak is ascribed to the release of water chemically bound to the material. For the sake of comparison, material 2 showed a single step of mass loss (about 12–13% by mass) attributed to the loss of chemically bound water in a wider range 70–250 °C. As far as MgAl-CO₃ is concerned, once this process is ended, a noticeable mass loss (about 10% by mass) takes place up to 270 °C, with a strong almost symmetrical DTA peak, attributed to evolution of water bound with stronger bonds to the material. In this regard, the occurrence of dehydroxylation due to condensation of hydroxyl groups of the inner layers cannot be excluded, although this process usually takes place in a wider temperature range and ends at higher temperature (> 500 °C) [55].

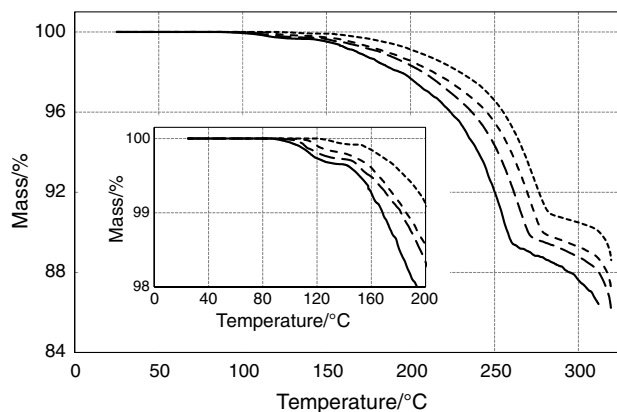


Fig. 5 Effect of sample mass on the TG curves at a heating rate of 5 K min⁻¹ under a flowing Ar atmosphere (60 mL min⁻¹). Sample size of about: 5 mg (—), 10 mg (— —), 15 mg (— —) and 20 mg (· · ·)

It is worth noting that more usually the shape and position of a TG curve may vary with the sample mass and the thickness of the sample particle layer [56]. It should be stressed that the sample mass may affect the TG curves depending on the type of reaction considered [55]. Figure 5 shows four TG curves carried out with different sample sizes (ranging from about 5 to 20 mg).

A systematic shift toward higher temperature is evident with increasing the sample size for each of the two processes accompanied by the evolution of water differently bound to the material. This behavior is attributed to a significant interaction between the vapor product in each process (water) and either the corresponding solid reactant or the solid product, like it was found for the thermal dehydration of calcium oxalate monohydrate [55].

Kinetic analysis of dehydration and decomposition

According to the scheme reported in Fig. S2, the kinetic analysis of both dehydration and decomposition was performed by processing DTA data related to both processes and determining the degree of conversion α from the fractional area. To this end, the original DTA curves at the five different heating rates from 1 to 9 °C min⁻¹ (Fig. S3a, Supplementary Materials) were corrected for the baseline drift and the corresponding α vs. T curves were constructed (Fig. S3b).

Once the isoconversional temperatures were determined for both the two steps, the activation energy is calculated at each given degree of conversion from the slopes of the KAS and incremental isoconversional Simon equations (according to Eqs. 6 and 7, respectively). The isoconversional dependence of activation energy of both processes is reported in Fig. 6 (plots a and b, respectively).

Activation energy for the first step shows in Fig. 6a a slight decreasing trend (from 83 to 72 kJ mol⁻¹), although practical constant values can be considered (within the estimated uncertainties expressed as error bars) and an average value of (69 ± 10) kJ mol⁻¹ can be evaluated in the range 0.1 < α < 0.9. These values are higher than that of the molar evaporation enthalpy of pure water at 100 °C (40.65 kJ mol⁻¹, as recalculated from [57]), thus demonstrating that a significant interaction takes place between water bound to the material and the material itself, as indicated by the results of the thermal behavior study (temperature shift with increasing the sample size). The corresponding dependence of pre-exponential factor is determined for both the first and second steps from the conversion dependence of activation energy of dehydration using the incremental isoconversional method (Eq. (8)), and the values are reported in Fig. S4 (plots a and b, Supplementary Material) with the associated uncertainties as error bars.

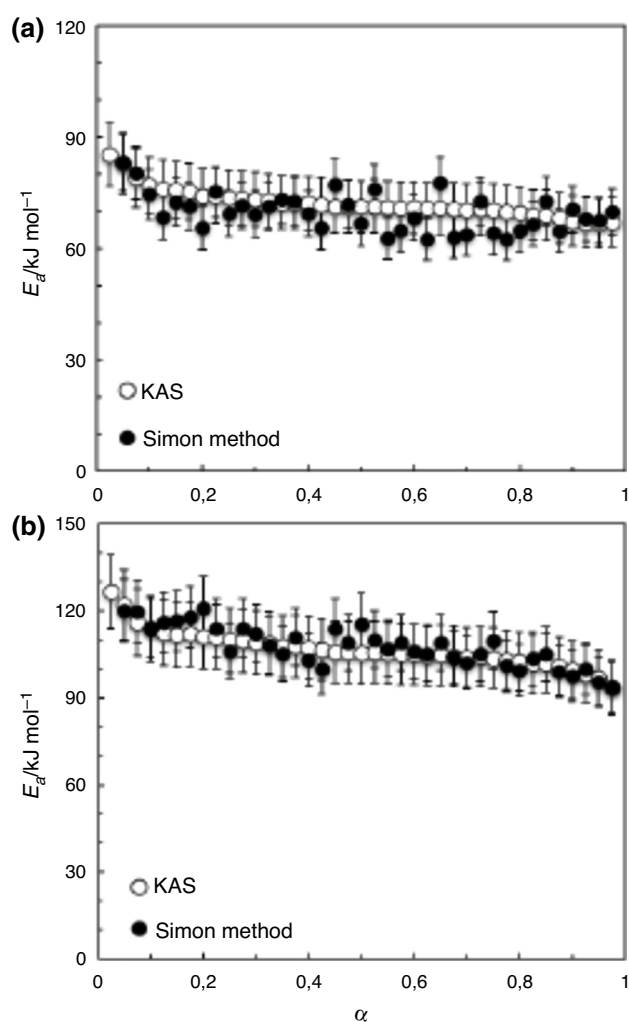


Fig. 6 Isoconversional E vs. α plots related to the first (a) and second (b) degradation steps of MgAl-CO₃

Table 1 Estimated and extrapolated reaction time values at fixed constant temperatures for given degree of conversions using isoconversional Arrhenius kinetic parameters related to the first step derived by the incremental isoconversional method (Eq. (8))

α	$\Delta t_{\text{calculated}}/\text{min}$			$\Delta t_{\text{extrapolated}}/\text{days}$	
	150 °C	120 °C	90 °C	37 °C	25 °C
0.05	0.5	2.3	14.2	0.6	1.7
0.10	1.4	5.6	29.2	0.9	2.5
0.50	5.8	25	136	4.6	13.4

As it is currently recognized by several authors [45, 47], neither the activation energy nor the pre-exponential factor can be considered alone as a stability parameter. However, using both the Arrhenius pair mean values derived by the incremental isoconversional Simon method (Eq. (7)), reasonable reaction time values are obtained according to

Eq. (8) at 90, 120 and 150 °C. These values are reported in Table 1 along with those extrapolated outside the experimental temperature range at 25 and 37 °C (value corresponding to the temperature of human body). Just for the sake of example, it was possible to reasonably predict that 50% of water (which is a very small amount) is released from the LDH material tested at 37 °C in about 5 days (4 days and 14 h) and at 25 °C in 13 days and 10 h.

A similar decreasing trend is observed in Fig. 6b for the E vs. a plot related to the second step with values ranging from 121 to 98 kJ mol⁻¹ and also in this case almost constant values can be considered within the estimated uncertainties and a mean value of (106 ± 7) kJ mol⁻¹ can be estimated in the range of a between 0.1 and 0.9. The dependence of pre-exponential factor is calculated through Eq. (8) from the conversion dependence of activation energy related to the second step using the incremental isoconversional method

Table 2 Estimated and extrapolated reaction time values at fixed constant temperatures for given degree of conversions using isoconversional Arrhenius kinetic parameters related to the second step derived by the incremental isoconversional method (Eq. (8))

α	$\Delta t_{\text{calculated}}/\text{min}$			$\Delta t_{\text{extrapolated}}/\text{years}$	
	200 °C	180 °C	150 °C	37 °C	25 °C
0.05	6	18	116	7	32
0.10	13	37	220	10	47
0.50	55	168	1119	105	556

and the corresponding values reported in Fig. S3b (Supplementary Material) with the associated uncertainties as error bars. From the Arrhenius pair determined by the Simon method for the second step, extremely high reaction time values were calculated using Eq. (8). Reaction time values of step 2 listed in Table 2 ranged from 10 to 40 times higher than those related to the first step resulting in a significant and probably unrealistic prediction of high stability: about 100 and more than 500 years to reach 50% of degradation at 37 and 25 °C, respectively. This overestimation of stability can be reasonably predicted also by considering that extrapolation outside the temperature range explored could be taken into account with care, since for reliable results kinetic parameters related to step 2 should hold for low temperatures, which are outside the measured range. In other words, the larger is the difference between measured and estimated temperature, the worse are prediction of stability made using kinetic parameters of decomposition.

Antimicrobial analysis

The antimicrobial properties of this material were investigated to check its potential ability to inhibit the growth of

the pathogenic bacterial strains, according to Kirby–Bauer method: the zone in which no growth has occurred is called inhibition halo. Also, according to Kirby–Bauer method, the bacterium is defined as resistant (R) if the diameter of the inhibition halo is equal to or less than 17 mm; intermediate (I) if the diameter is between 18 and 22 mm; sensitive (S) if it is equal to or greater than 23 mm. As observed from representative image of petri plate (Fig. 7), no inhibition halo was observed and 100% of bacterial viability was observed for the MgAl-CO₃ tested with four different strains. The bacterial resistance to the synthesized material could be explained by the inability of the material to release metal ions at toxic concentration. Indeed, many authors support the idea that metal ions at higher concentration have a negative effect on the microbial growth [58, 59].

Conclusions

The thermal behavior and the antibacterial properties of the layered MgAl-CO₃, synthesized were analyzed along with its structural and morphological characteristics with XRPD and FESEM measurements, respectively. The compound has been synthesized via a co-precipitation route (direct method) followed by an hydrothermal treatment, and a partially disordered structure was observed, which is characterized by the presence of crystallites with a nanoscopic size. The antibacterial tests carried out in this study demonstrated the inability of the layered MgAl-CO₃ to inhibit the growth of the pathogenic bacterial strains, according to the Kirby–Bauer method. The results of the thermal behavior study, through the TG and DTA experiments revealed that a noticeable interaction takes place between water (in the vapor phase) and MgAl-CO₃ in both processes. Kinetic analysis of both steps (according to either isoconversional integral and incremental isoconversional methods) provides almost constant values of activation energy, whose mean values in the range 0.1 < a < 0.9 are: $E_1 = (66 \pm 9)$ kJ mol⁻¹; $E_2 = (106 \pm 7)$ kJ mol⁻¹. Finally, reaction times were reasonably predicted by extrapolation at 25 and 37 °C using kinetic parameters of the first step and can be used for assessment of thermal stability. Conversely, the same procedure adopted by using the kinetic parameters related to the second step seems to provide almost unrealistic reaction time values.

Supplementary Information The online version contains supplementary material available at <https://doi.org/10.1007/s10973-022-11334-3>.

Author contributions All authors contributed to the study conception and design. Material preparation, data collection and analysis were performed by [Anna Maria Cardinale], [Marco Fortunato]. The first and the revised versions of the manuscript were written by all authors. All authors read and approved the final revised version of the manuscript.

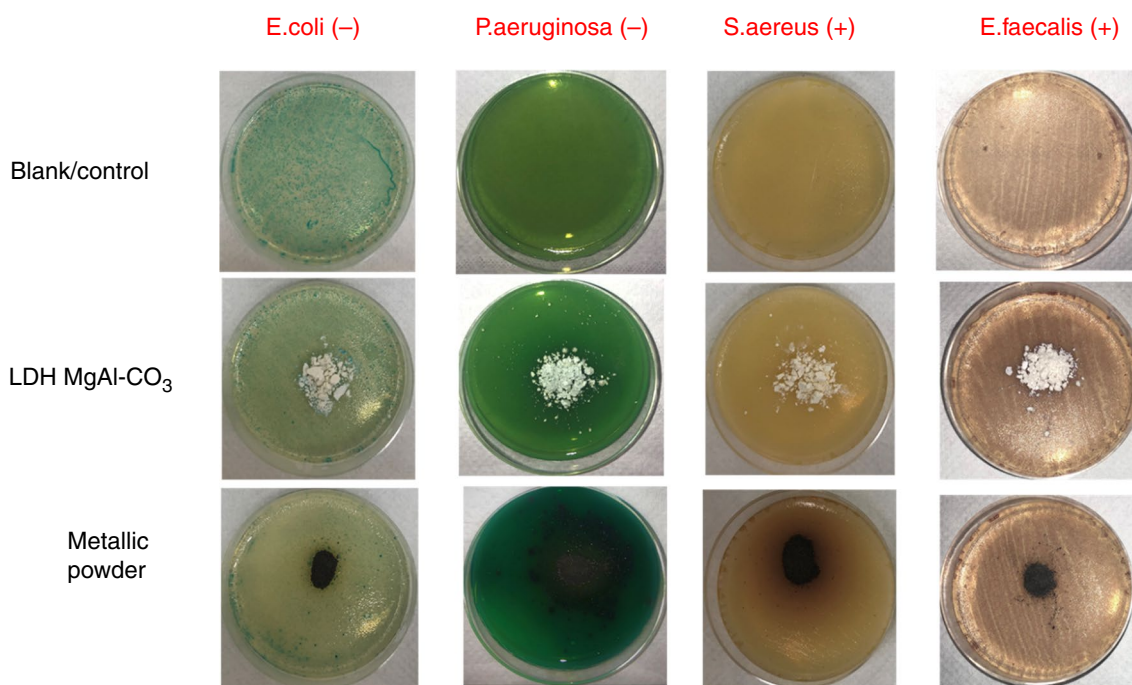


Fig. 7 Representative images of the sample with respect to the control

Open Access This article is licensed under a Creative Commons Attribution 4.0 International License, which permits use, sharing, adaptation, distribution and reproduction in any medium or format, as long as you give appropriate credit to the original author(s) and the source, provide a link to the Creative Commons licence, and indicate if changes were made. The images or other third party material in this article are included in the article's Creative Commons licence, unless indicated otherwise in a credit line to the material. If material is not included in the article's Creative Commons licence and your intended use is not permitted by statutory regulation or exceeds the permitted use, you will need to obtain permission directly from the copyright holder. To view a copy of this licence, visit <http://creativecommons.org/licenses/by/4.0/>.

References

- Cavani F, Trifirò F, Vaccari A. Hydrotalcite-type anionic clays: Preparation, properties and applications. *Cat Today*. 1991. [https://doi.org/10.1016/0920-5861\(91\)80068-K](https://doi.org/10.1016/0920-5861(91)80068-K).
- Zümreoglu B, Ay AN. Layered double hydroxides — multifunctional nanomaterials. *Chem Papers*. 2012;66(1):1–10. <https://doi.org/10.2478/s11696-011-0100-8>.
- Ahmed N, Shibata Y, Taniguchi T, Izumi Y. Photocatalytic conversion of carbon dioxide into methanol using zinc-copper-M(III) (M = aluminum, gallium) layered double hydroxides. *J Catal*. 2011;279:123–35. <https://doi.org/10.1016/j.jcat.2011.01.004>.
- Patel R, Park JT, Patel M, Dash JM, Gowd EB, Karpoornath R, Mishra A, Kwak J, Kim JH. Transition-metal-based layered double hydroxides tailored for energy conversion and storage. *J Mater Chem A*. 2017;6:12–29. <https://doi.org/10.1039/C7TA09370E>.
- Lai F, Miao YE, Zuo L, Lu H, Huang Y, Liu T. Biomass-derived nitrogen doped carbon nanofiber network: a facile template for decoration of ultrathin nickel-cobalt layered double hydroxide nanosheets as high-performance asymmetric supercapacitor electrode. *Small*. 2016;12:3235–44. <https://doi.org/10.1002/smll.201600412>.
- Cardinale AM, Carbone C, Consani S, Fortunato M, Parodi N. Layered double hydroxides for remediation of industrial wastewater from a galvanic plant. *Curr Comput-Aided Drug Des*. 2020;10(6):443. <https://doi.org/10.3390/cryst10060443>.
- Zhao J, Zhang L, Zhang S, Yuan W, Fang X, Yu Q, Qiu X. Remediation of chromium-contaminated soil using calcined layered double hydroxides containing different divalent metals: Temperatures and mechanism. *Chem Eng J*. 2021;425: 131405. <https://doi.org/10.1016/j.cej.2021.131405>.
- Li X, Fortunato M, Cardinale AM, Sarapulova A, Njel C, Dsoke S. Electrochemical study on nickel aluminum layered double hydroxides as high-performance electrode material for lithium-ion batteries based on sodium alginate binder. *J Solid State Electrochem*. 2021. <https://doi.org/10.1007/s10008-021-05011-y>.
- Domingues M, de Sousa AL, dos Santos WM, de Souza ML, Barreto Barros Silva LCP, Eun He Koo Yun A, Siqueira Britto Aguilera C, de França CB, Araújo Rolim L, MariaFerreira da Silva R, José Rolim Neto P. Layered double hydroxides as promising excipients for drug delivery purposes. *Eur J Pharm Sci*. 2021;165:105922. <https://doi.org/10.1016/j.ejps.2021.105922>.
- Rahman MT, Kameda T, Miura T, Kumagai S, Yoshioka T. Removal of sulfate from wastewater via synthetic Mg–Al layered double hydroxide: An adsorption, kinetics, and thermodynamic study. *J Indian Chem Soc*. 2021;98(11): 100185. <https://doi.org/10.1016/j.jics.2021.100185>.
- Jin W, Park D-H. Functional layered double hydroxide nano-hybrids for biomedical imaging. *Nanomaterials*. 2019;9:1404. <https://doi.org/10.3390/nano9101404>.
- Kargozar S, Montazerian M, Hamzehlou S, Kim H-W, Baino F. Mesoporous bioactive glasses: Promising platforms for

- antibacterial strategies. *Acta Biomater.* 2014;10(8):1–19. <https://doi.org/10.1016/j.actbio.2018.09.052>.
13. Montazerian M, Yekta BE, Marghussian VK, Bellani CF, Siqueira RL, Zanutto ED. Bioactivity and cell proliferation in radiopaque gel-derived CaO–P₂O₅–SiO₂–ZrO₂ glass and glass–ceramic powders. *Mater Sci Eng C.* 2015;55:436–47. <https://doi.org/10.1016/j.msec.2015.05.065>.
 14. Magri VR, Duarte A, Perotti GF, Constantino VRL. Investigation of thermal behavior of layered double hydroxides intercalated with carboxymethylcellulose aiming bio-carbon based nanocomposites. *Chem Eng.* 2019;3:55. <https://doi.org/10.3390/chemengineering3020055>.
 15. Theiss FL, Ayoko GA, Frost RL. Thermogravimetric analysis of selected layered double hydroxides. *J Therm Anal Calorim.* 2013;112:649–57. <https://doi.org/10.1007/s10973-012-2584-z>.
 16. Rives V, editor. Layered double hydroxides: present and future. New York: Nova Science Pub Inc; 2001.
 17. Rives V. Characterisation of layered double hydroxides and their decomposition products. *Mater Chem Phys.* 2002;75:19–25. [https://doi.org/10.1016/S0254-0584\(02\)00024-X](https://doi.org/10.1016/S0254-0584(02)00024-X).
 18. Kanazaki E. Thermal behavior of the hydrotalcite-like layered structure of Mg and Al-layered double hydroxides with interlayer carbonate by means of in situ powder HTXRD and DTA/TG. *Solid State Ionics.* 1998;106(3–4):279–84. [https://doi.org/10.1016/S0167-2738\(97\)00494-3](https://doi.org/10.1016/S0167-2738(97)00494-3).
 19. Vecchio Cipriotti S, Catauro M. Synthesis, structural and thermal behavior study of four Ca-containing silicate gel-glasses: activation energies of their dehydration and dehydroxylation processes. *J Therm Anal Calorim.* 2016;123:2091–101.
 20. Zhu H, Boccaccini AR. Biologically active ions and therapeutic biomolecules. *Acta Biomater.* 2021;129:1–17. <https://doi.org/10.1016/j.actbio.2021.05.007>.
 21. Pouroutzidou GK, Theodorou GS, Kontonasaki E, Tsamesidis I, Pantaleo A, Patsiaoura D, Papadopoulou L, Rhoades J, Likotraftiti E, Lioutas CB, Chrissafis K, Paraskevopoulos KM. Effect of ethanol/TEOS ratios and amount of ammonia on the properties of copper-doped calcium silicate nanoceramics. *J Mater Sci Mater Med.* 2019. <https://doi.org/10.1007/s10856-019-6297-8>.
 22. Vecchio Cipriotti S, Bollino F, Tranquillo E, Catauro M. Synthesis, thermal behavior and physico-chemical characterization of ZrO₂/PEG inorganic/organic hybrid materials via sol-gel technique. *J Therm Anal Calorim.* 2017;130:535–40. <https://doi.org/10.1007/s10973-017-6318-0>.
 23. Catauro M, Papale F, Bollino F, Piccolella S, Marciano S, Nocera P, Pacifico S. Silica/quercetin sol–gel hybrids as antioxidant dental implant materials. *Sci Technol Advanced Mater.* 2015;16:3. <https://doi.org/10.1088/1468-6996/16/3/035001>.
 24. Ognibene G, Cristaldi DA, Fiorenza R, Blanco I, Cicala G, Scirè S, Fragalà ME. Photoactivity of hierarchically nanostructured ZnO–PES fibre mats for water treatments. *RSC Adv.* 2016;49(6):42778–85. <https://doi.org/10.1039/C6RA06854E>.
 25. Milia A, Bruno M, Cavallaro G, Lazzara G, Milioto S. Adsorption isotherms and thermal behavior of hybrids based on quercetin and inorganic fillers. *J Therm Anal Calorim.* 2019;138:1971–7. <https://doi.org/10.1007/s10973-019-08257-x>.
 26. Catauro M, Bollino F. Anti-inflammatory entrapment in polycaprolactone/silica hybrid material prepared by sol-gel route, characterization, bioactivity and in vitro release behavior. *J Appl Biomater Funct Mater.* 2013;11(3):172–9. <https://doi.org/10.5301/JABFM.2012.9256>.
 27. Catauro M, Dal Poggetto G, Sgarlata C, Vecchio Cipriotti S, Pacifico S, Leonelli C. Thermal and microbiological performance of metakaolin-based geopolymers cement with waste glass. *Appl Clay Sci.* 2020;197: 105763. <https://doi.org/10.1016/j.clay.2020.105763>.
 28. Theodorou G, Kontonasaki E, Theocharidou A, Bakopoulou A, Bounaki M, Hadjichristou C, Papachristou E, Papadopoulou L, Kantiranis N, Chrissafis K, Paraskevopoulos K, Paraskevopoulos K, Koidis P. Sol-gel derived mg-based ceramic scaffolds doped with zinc or copper ions: preliminary results on their synthesis, characterization, and biocompatibility. *Int J Biomater.* 2016;2016:1–11. <https://doi.org/10.1155/2016/3858301>.
 29. Calvino MM, Lisuzzo L, Cavallaro G, Lazzara G, Milioto S. Non-isothermal thermogravimetry as an accelerated tool for the shelf-life prediction of paracetamol formulations. *Thermochim Acta.* 2021;700: 178940. <https://doi.org/10.1016/j.tca.2021.178940>.
 30. Lisuzzo L, Caruso MR, Cavallaro G, Milioto S, Lazzara G. Hydroxypropyl cellulose films filled with halloysite nanotubes/wax hybrid microspheres. *Ind Eng Chem Res.* 2021;60(4):1656–65. <https://doi.org/10.1021/acs.iecr.0c05148>.
 31. Blanco I. Polysiloxanes in theranostics and drug delivery: A review. *Polymers.* 2018;10(7):755. <https://doi.org/10.3390/polym10070755>.
 32. Vecchio S, Rodante F, Tomassetti M. Thermal stability of disodium and calcium fosfomycin and the effects of the excipients evaluated by thermal analysis. *J Pharm Biomed Anal.* 2001;24:1111–23. [https://doi.org/10.1016/s0731-7085\(00\)00568-9](https://doi.org/10.1016/s0731-7085(00)00568-9).
 33. Papadopoulos C, Cristóvão B, Ferenc W, Hatzidimitriou A, Vecchio Cipriotti S, Risoluti R, Lalia-Kantouri M. Thermoanalytical, magnetic and structural investigation of neutral Co(II) complexes with 2,2'-dipyridylamine and salicylaldehydes. *J Therm Anal Calorim.* 2016;123:717–29. <https://doi.org/10.1007/s10973-015-4976-3>.
 34. Zianna A, Vecchio S, Gdaniec M, Czapik A, Hatzidimitriou A, Lalia-Kantouri M. Synthesis, thermal analysis, spectroscopic and structural characterization of zinc(II) complexes with salicylaldehydes. *J Therm Anal Calorim.* 2013;112:455–64. <https://doi.org/10.1007/s10973-012-2719-2>.
 35. Papadopoulos C, Kantiranis N, Vecchio S, Lalia-Kantouri M. Lanthanide complexes of 3-methoxy-salicylaldehyde: thermal investigation by simultaneous TG/DTG-DTA coupled with MS; Thermal decomposition kinetics. *J Therm Anal Calorim.* 2010;99:931–8. <https://doi.org/10.1007/s10973-009-0640-0>.
 36. Vecchio S, Materazzi S, Wo LW, De Angelis CS. Thermoanalytical study of imidazole-substituted coordination compounds: Cu(II)- and Zn(II)-complexes of bis(1-methylimidazol-2-yl) ketone. *Thermochim Acta.* 2013;568:31–7. <https://doi.org/10.1016/j.tca.2013.06.016>.
 37. Rao MM, Reddy BR, Jayalakshmi M, Jaya VS, Sridhar B. Hydrothermal synthesis of Mg–Al hydrotalcites by urea hydrolysis. *Mat Res Bull.* 2005. <https://doi.org/10.1016/j.materresbull.2004.10.007>.
 38. Villarks P, Cenxual K. Pearson's Crystal Data- Crystal Structure Database for Inorganic Compounds, Release 2017/18, ASM international, Materials Park, Ohio, USA.
 39. King G, Schwarzenbach LD., Xtal3.7 system, In: Hall SR, du Boilay DJ, Olthof-Hazekamp R, editors. *Crawley: University of Western; 2000.*
 40. Catauro M, D'Errico Y, D'Angelo A, Clarke RJ, Blanco I. Antibacterial activity and iron release of organic-inorganic hybrid biomaterials synthesized via the sol-gel route. *Appl Sci.* 2021;11(19):9311. <https://doi.org/10.3390/app11199311>.
 41. Dal Poggetto G, Catauro M, Crescente G, Leonelli C. Efficient addition of waste glass in MK-based geopolymers: microstructure, antibacterial and cytotoxicity investigation. *Polymers.* 2021;13(9):1493. <https://doi.org/10.3390/polym13091493>.
 42. Rodante F, Vecchio S, Catalani G, Guidotti M. Thermal analysis and non-isothermal kinetic study of some pesticides. Part II Chlorinate derivatives. *J Therm Anal Calorim.* 2000;60:605–22. <https://doi.org/10.1023/A:1010159424733>.

43. Doyle CD. Estimating isothermal life from thermogravimetric data. *J Appl Polym Sci.* 1962;6(24):639–42. <https://doi.org/10.1002/app.1962.070062406>.
44. Akahira T, Sunose T. Paper No. 246, 1969 research report, trans. joint convention of four electrical institutes. *Chiba Inst Technol (Sci Technol).* 1971;16:22–31.
45. Dubai T, Cibulková Z, Šimon P. An incremental isoconversional method for kinetic analysis based on the orthogonal distance regression. *J Comput Chem.* 2015;36:392–8. <https://doi.org/10.1002/jcc.23813>.
46. Šimon P, Thomas P, Dubai T, Cibulková Z, Peller A, Veverka M. The mathematical incorrectness of the integral isoconversional methods in case of variable activation energy and the consequences. *J Therm Anal Calorim.* 2014;115:853–9. <https://doi.org/10.1007/s10973-013-3459-7>.
47. Budrugaec P, Homentcovschi D, Segal E. Critical analysis of the isoconversional methods for evaluating the activation energy. III. On the evaluation of the activation energy from non-isothermal data. *J Therm Anal Calorim.* 2001;66:557–65. <https://doi.org/10.1023/A:1010148611036>.
48. Vyazovkin S. Modification of the integral isoconversional method to account for variation in the activation energy. *J Comput Chem.* 2001;22:178–83. <https://doi.org/10.1002/1096-987X>.
49. Fukumoto T, Thomas P, Šimon P, Dubai T, Stuart B. Estimation of the curing rate of acrylamide used as a consolidant in heritage sandstone conservation. *J Therm Anal Calorim.* 2014;116:619–24. <https://doi.org/10.1007/s10973-014-3730-6>.
50. Rodriguez-Carvajal J. FULLPROF: A Program for Rietveld Refinement and Pattern Matching Analysis. Abstracts of the Satellite Meeting on Powder Diffraction of the XV Congress of the IUCr, 127, Toulouse, France, 1990.
51. Liao L, Zhao N, Xia Z. Hydrothermal synthesis of Mg-Al layered double hydroxides (LDHs) from natural brucite and Al(OH)₃. *Mat Res Bull.* 2012. <https://doi.org/10.1016/j.materresbull.2012.07.007>.
52. Li X, Wan G, Xiao J, Wu L, Shi S, Wang G. Carbon-coated Ni(OH)₂-NiAl LDH hierarchical nanostructures on Ni foam as a high areal capacitance electrode for supercapacitor application. *Mater Lett.* 2018;228:179–82. <https://doi.org/10.1016/j.matlet.2018.06.012>.
53. Boccalon E, Gorrasi G, Nocchetti M. Layered double hydroxides are still out in the bloom: Synthesis, applications and advantages of three-dimensional flower-like structures. *Adv Colloid Interface Sci.* 2020;285: 102284. <https://doi.org/10.1016/j.cis.2020.102284>.
54. Vyazovkin S, Chrissafis K, Di Lorenzo ML, Koga N, Pijolat M, Roduit B, Sbirrazzuoli N, Suñol JJ. experimental thermal analysis data for kinetic computations. *Thermochim Acta.* 2014;590:1–23. <https://doi.org/10.1016/j.tca.2014.05.036>.
55. Vecchio Cipriotti S, Catauro M, Bollino F, Tuffi R. Thermal behavior and dehydration kinetic study of SiO₂/PEG hybrid gel glasses. *Polym Eng Sci.* 2017;57(6):606–12. <https://doi.org/10.1002/polb.24561>.
56. Koga N, Tanaka H. Effect of sample mass on the kinetics of thermal decomposition of a solid. II. Isothermal dehydration of Li₂SO₄•H₂O. *J Therm Anal.* 1993;40:1173–9. <https://doi.org/10.1007/BF02546880>.
57. Kirkham MB, in *Principles of Soil and Plant Water Relations (Second Edition), Structure and Properties of Water*, Academic Press, Chapter 3, pp. 27–40, 2014. <https://doi.org/10.1016/B978-0-12-420022-7.00003-3>
58. Sheldon JR, Skaar EP. Metals as phagocyte antimicrobial effectors. *Curr Opin Immunol.* 2019;60:1–9. <https://doi.org/10.1016/j.coi.2019.04.002>.
59. Sharifi Y, Abedzadeh A, Salighe A, Kalhor N, Motlagh MK, Javadi A. Antibiotics and heavy metals resistance patterns of *Enterococcus faecalis* and *faecium* bacteria isolated from the human and the livestock sources. *Env Health Eng Manag J.* 2015;2(4):199–202.

Publisher's Note Springer Nature remains neutral with regard to jurisdictional claims in published maps and institutional affiliations.